Article

Not peer-reviewed version

Optoelectronic proprieties improvement of multicrystalline silicon by Alumina Nanoparticles and silicon nitride

Mohamed Ben Rabha *, Ameny El Haj, Achraf Mannai, Karim Choubani *, Mohammed A Almeshaal, Wissem Dimassi

Posted Date: 18 March 2025

doi: 10.20944/preprints202503.1252.v1

Keywords: multicrystalline silicon; porous silicon; alumina nanoparticles; silicon nitride; LBIC; diffusion length; surface reflectivity

 doi:10.20944/preprints202503.1252.v1

Article

Optoelectronic Proprieties Improvement of Multicrystalline Silicon by Alumina Nanoparticles and Silicon Nitride

Mohamed Ben Rabha [1,*], Amany El Haj [1], Achref Mannai [1], Karim Choubani [2,*], Mohammed A. Almeshaal [2] and Wissem Dimassi [1]

[1] Laboratoire de Nanomatériaux et Systèmes pour Énergies Renouvelables, Centre de Recherches et des Technologies de l'Énergie, Technopôle de Borj-Cédria, BP 95 Hammam-Lif, Tunis, 2050, Tunisie; amenyelhaj@gmail.com (A.E.H.); achref.mannai87@gmail.com (A.M.); dimassi.wissem@gmail.com (W.D.)
[2] College of Engineering, Imam Mohammad Ibn Saud Islamic University, Riyadh, Saudi Arabia; m_almeshaal@hotmail.com
* Correspondence: rabha2222@yahoo.fr (M.B.R.); kelchobani@imamu.edu.sa (K.C.)

Abstract: In this paper, we compared the effects of alumina nanoparticles and silicon nitride layer deposited on multi-crystalline silicon separately of structure, optic, and optoelectronic properties, to achieve excellent surface. Alumina nanoparticles -covered mc-Si immersion in $HF/H_2O_2/HNO_3$ and porous silicon covered with silicon nitride structure are the key factors to achieving a high electronic quality of multi-crystalline silicon. Consequently, the surface reflectivity decreases from 35% to 2% for alumina nanoparticles/PS and to 5% for silicon nitride/PS in the wavelength range of 250–1200 nm. Meanwhile, the minority carrier diffusion length increases from 2 μm to 300 μm for PS combined with SiNx and to 100 μm for alumina nanoparticles/PS. Furthermore, the Two-Dimensional Produced Current measurement shows a significant enhancement compared to bare mc-Si (2.8 nA), reaching a maximum of 34 nA for alumina nanoparticles/PS and 66 nA for PS combined with SiN. These results indicate that multi-crystalline silicon surface passivation using aluminum/PS or PS combined with SiNx is an effective approach to enhancing the electronic quality of mc-Si wafers, thereby improving the efficiency of mc-Si-based solar cells.

Keywords: multicrystalline silicon; porous silicon; alumina nanoparticles; silicon nitride; LBIC; diffusion length; surface reflectivity

1. Introduction

Multicrystalline silicon (mc-Si) is a prevalent material in solar cell production due to its cost-effectiveness and reasonable efficiency [1,2]. However, its electronic quality often suffers from defects, impurities, and grain boundaries, limiting performance [3–5]. Recent studies have explored silicon nitride [6] and alumina nanoparticles [7] to enhance the electronic properties of mc-Si. Mc-Si comprises multiple silicon crystals, leading to a heterogeneous structure that can negatively impact charge carrier mobility and recombination rates. Defects in mc-Si, such as dislocations and grain boundaries [8,9], are known to act as recombination centers, reducing overall efficiency. silicon nitride is widely used as a passivation layer in solar cells due to its excellent dielectric properties and ability to reduce surface recombination. The incorporation of silicon nitride and alumina nanoparticles [10] creates a barrier that prevents minority carrier recombination at the silicon surface, thus enhancing charge carrier lifetime. Lowering the surface reflectance of silicon wafers through porous silicon (PS) [11,12] treatment is a key process for enhancing the efficiency of silicon solar cells. The formation of PS via stain etching (SE) [13] is a suitable approach for the photovoltaic industry, as it requires only a short immersion of the substrates in an appropriate solution [13]. In a previous study, we reported that SE of the silicon substrate leads to a significant reduction in surface reflectance [14]. This is of great importance for silicon-based solar cells due to the sunlight absorption improvement. On the other hand, the alumina nanoparticles /PS and silicon-nitride (SiNx)/PS could act not only as an antireflection coating (ARC), but also to improve the performance of photovoltaic devices by defect, surface, and bulk passivation. This study aims to demonstrate the enhancement of surface

 doi:10.20944/preprints202503.1252.v1

passivation and electronic quality in mc-Si through the use of aluminum/porous silicon nanostructures and PS combined with SiNx. alumina nanoparticles-covered mc-Si immersion in $HF/H_2O_2/HNO_3$ and mc-Si immersion in $HF/H_2O_2/HNO_3$ covered with silicon nitride deposited by plasma enhanced chemical vapor deposition (PECVD) were characterized to investigate the structure optic and optoelectronic properties by measuring reflectance, IR absorption, lifetime, and laser beam-induced current (LBIC).

2. Materials and Methods

A p-type mc-Si wafer with a thickness of 350 μm and a resistivity of 2.0-0.5 Ω cm was used in this work. Porous silicon layers were accomplished by stain etching method at room temperature using a mixed solution containing H_2O: HNO_3: HF in the ratio of 5:3:1. The solution was agitated to prevent H_2 from bubbling over the etching surface and thus, fabricate a more uniform PS structure. The sample with alumina nanoparticles was treated in HF: HNO_3: H_2O solution for a few seconds to obtain the silicon nanostructures, while the mc-Si treated in HF: HNO_3: H_2O solution was covered with a SiN_x thin films using a Plasma-Enhanced Chemical Vapor Deposition (PECVD) by decomposition of silane SiH_4 and H_2. The samples' surface morphology was observed by scanning electron microscope. UV–vis–NIR spectrophotometer (Perkin-Elmer Lambda 950) equipment measured reflectance with an integrating sphere in the 250–1200 nm wavelength range. Fourier transform infrared (Nicolet MAGNA-IR 560 ESP FT-IR) analysis was used to estimate bond densities in the elaborated samples. The minority carriers' diffusion length was determined by the Light Beam Induced Current (LBIC) system to quantify the electronic quality of the treated mc-Si.

3. Results and discussion

Figure 1 shows an SEM morphology of mc-Si. Top-view SEM images provide valuable insights into the structural features, grain boundaries, and surface conditions that influence the electronic properties of mc-Si, which is critical for solar cell applications.

SEM micrographs of ref mc-Si reveal a mosaic-like structure characterized by distinct grains of varying sizes (Figure 1(a)). The grain sizes significantly affect the electronic properties of mc-Si. Larger grains generally lead to improved charge carrier mobility and reduced recombination rates. Variability in grain size indicates the quality of the crystallization process during manufacturing. Uniform grain sizes are often associated with higher-quality material. Figure 1(a)) shows varying degrees of surface roughness, which is influenced by the fabrication methods and the subsequent texturing processes. The increased surface roughness enhances light absorption by reducing reflectivity, which is beneficial for solar cell efficiency. However, excessive roughness may lead to increased defect densities and surface states, potentially harming electronic performance. The grain boundaries are visible, appearing as lines or interfaces separating different crystalline regions. These boundaries act as recombination centers for charge carriers, negatively affecting the efficiency of mc-Si solar cells. Understanding the distribution and characteristics of grain boundaries is crucial for improving the electronic quality of the material. Figure 1 (b) shows alumina nanoparticules dispersion on a mc-Si surface. Top-view Scanning Electron Microscopy (SEM) images provide crucial insights into the dispersion, morphology, and interactions of aluminum nanoparticles with the mc-Si surface. The obtained results reveal the distribution pattern of aluminum nanoparticles across the mc-Si surface. A uniform dispersion of nanoparticles is desirable, as it can enhance optical and electrical properties of mc-Si. Clusters or agglomerations of nanoparticles may indicate issues during the deposition process, potentially leading to uneven light scattering and localized recombination sites. An even distribution can improve light trapping and enhance the overall absorption efficiency of the solar cell.

 doi:10.20944/preprints202503.1252.v1

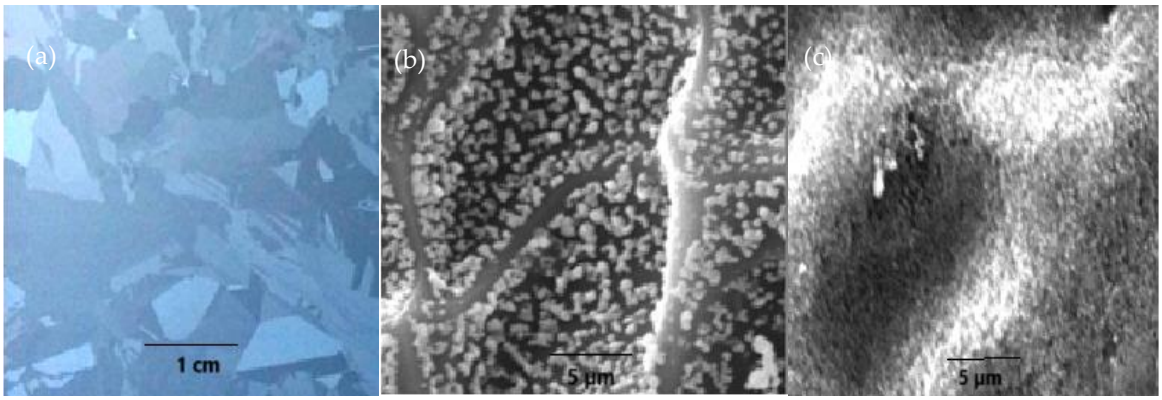

Figure 1. SEM morphology of mc-S: (a) Ref mc-Si wafer (b) Al-NPs dispersion (c) mc-Si with Al-NPs after HF/H_2O_2/HNO_3 treatment.

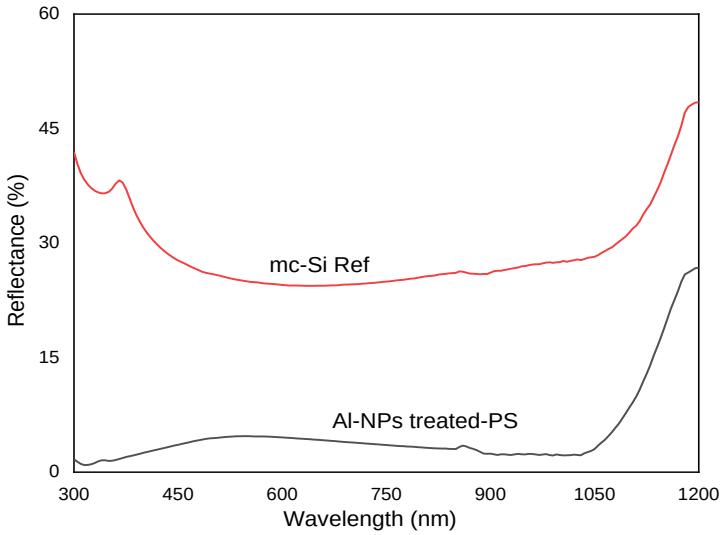

Figure 2. Total reflectance before and after silicon nanostructure formation.

The SEM images may show the size, shape, and morphology of the aluminum nanoparticles. Successful integration of aluminum nanoparticles leads to improved surface passivation, reducing surface recombination rates of charge carriers. The interface between the nanoparticles and the mc-Si surface is critical. Effective bonding enhances charge carrier collection, while weak interactions may lead to increased recombination. Aluminum nanoparticles enhance light trapping through scattering and absorption mechanisms, which may not be directly visible in SEM images but can be inferred from the dispersion quality and morphology. Figure 1(c) shows the mc-Si-covered Al Nanoparticles after HF/H_2O_2/HNO_3 treatment. Top-view Scanning Electron Microscopy (SEM) provides critical insights into the morphological changes and dispersions of aluminum nanoparticles on the mc-Si surface after such treatments. The HF treatment effectively removes native silicon oxide layers, resulting in a cleaner silicon surface that may enhance the adhesion of aluminum nanoparticles.

The subsequent H_2O_2 and HNO_3 treatments oxidize the aluminum nanoparticles, potentially altering their size and morphology, leading to more uniform dispersions. The chemical treatments not only modify the nanoparticles but also affect the mc-Si surface itself, potentially increasing surface area and improving light trapping. Enhanced surface passivation may result from the interaction between the aluminum nanoparticles and the silicon surface, reducing recombination rates and improving charge carrier dynamics. The combination of cleaning and nanoparticle dispersion is likely to enhance the effective utilization of incident light, which is essential for improving the efficiency of solar cells.

The surface reflectance of mc-Si with and without Al-NPS treated by PS are shown in Figure 2. From the reflectivity spectra, it is clear that the average reflectivity of Al-NPS treated by PS is significantly lower than that of the bare mc-Si sample in the 300–1200 nm range. The reflectivity of the silicon surface decreases to below 4% for most wavelengths in the spectrum (between 450 and 1050 nm), and further drops to 2% in the lower wavelength range (300–450 nm). This indicates that the

 doi:10.20944/preprints202503.1252.v1

silicon nanostructures formed after Al-NPS treated by PS enhance light absorption, with the lowest reflectivity being attributed to the formation of mc-Si nanostructures that are suitable for light trapping due to multiple reflections [15–18]. It's well known that mc-Si-NS mainly absorb short-wavelength incident light. The SEM morphology shown in Figure 1(c) confirms the existence of nanostructures formed by pores of varying dimensions and supports the light trapping structure observed in Figure 2, as indicated by the reduction in reflectivity, as suggested by [19]. Figure 3 shows a typical SEM micrograph (top view) of PS covered with silicon nitride. The top-view SEM images typically reveal the porous structure of the silicon, characterized by a network of interconnected pores. The morphology of PS is crucial as it influences light trapping and overall optical properties. The well-porous structure enhances light absorption via scattering effects. The modification of the PS surface with SiNx results in changes in reflectivity and light absorption characteristics, which not be directly visible in SEM but can be inferred from the morphology. The SiNx layer enhances the optical properties of PS by reducing surface reflectance and improving light absorption. Understanding the interaction between the SiNx layer and the porous structure helps in designing devices with optimized light management properties.

The surface morphology is homogeneous and exhibits an irregular structure, which may be suitable for light trapping and diffusion. The optical reflectivity of this structure decreases dramatically to about 5%, compared to both untreated and PS-treated mc-Si (Figure 3a). This can be explained, as previously reported [16], by the increase in surface roughness.

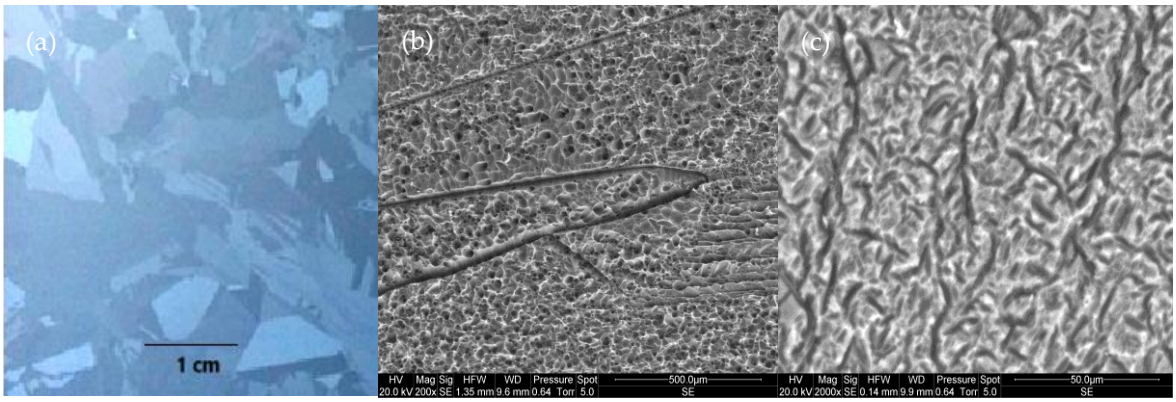

Figure 3. SEM image of mc-Si (a) ref sample (b) PS and (c) PS covered with SiN.

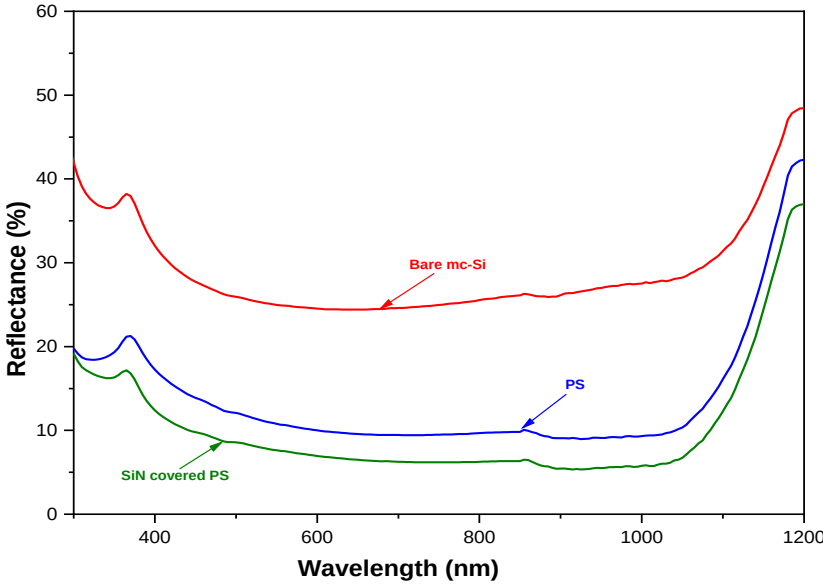

Figure 4. Reflectivity characteristics of mc-Si: (a) ref, (b) PS (c) PS/SiN.

A comparison of mc-Si-treated PS and mc-Si-treated PS Covered-SiN shows some benefits. First, mc-Si-treated PS Covered-SiN is formed homogeneously on the entire area of the mc-Si surface

 doi:10.20944/preprints202503.1252.v1

without obstruction of the grain orientation. Second mc-Si-treated PS Covered-SiN demonstrated optical concert greater than the mc-Si-treated PS layers. Also, PS and SiN have some passivating capabilities, which allow the fabricated solar cells without an additional passivation coating.

To quantify the electronic quality of mc-Si substrates treated with PS-covered SiN and alumina nanoparticles, optoelectronic properties were studied using two methods: diffusion length and produced current surface distribution. The diffusion length of alumina nanoparticles-covered mc-Si, as measured [20,21], increased drastically from 2 μm for the bare sample to 100 μm for Al-NPS treated by PS. This significant increase suggests that the enhanced diffusion length and improved surface quality are primarily attributed to the passivation effect of the Al-oxide species and the reduction in surface recombination velocity, likely due to aluminum gettering [22] (Al diffuses and penetrates the material in the phase of the annealing and able to remove). Which was approved by FTIR characterization as shown in Figure 5.

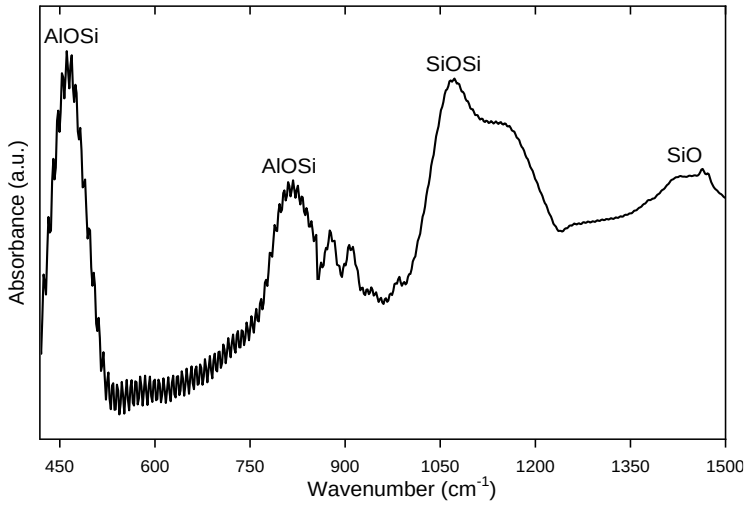

Figure 5. FT-IR characterization of Al-NPS Treated PS.

As shown in Figure 5, the peaks at 810 and 460 cm^{-1} are attributed to the stretching mode of AlOSi [19]. Notably, these peaks align well with those reported in previous literature [23–28]. The SiO and AlOSi species generated by Al-NPS treated with PS structures help passivate the defects and dangling bonds at the interface and grain boundaries (GBs) of multi-crystalline silicon samples. In contrast, for PS covered with SiNx, the diffusion length of minority carriers increased from 2 μm in bare mc-Si to 300 μm in PS-covered SiNx. This improvement is attributed to the passivation of defects in mc-Si by the penetrated hydrogen, leading to an overall enhancement in the quality of mc-Si for solar cell applications, as confirmed by FTIR characterization, shown in Figure 6.

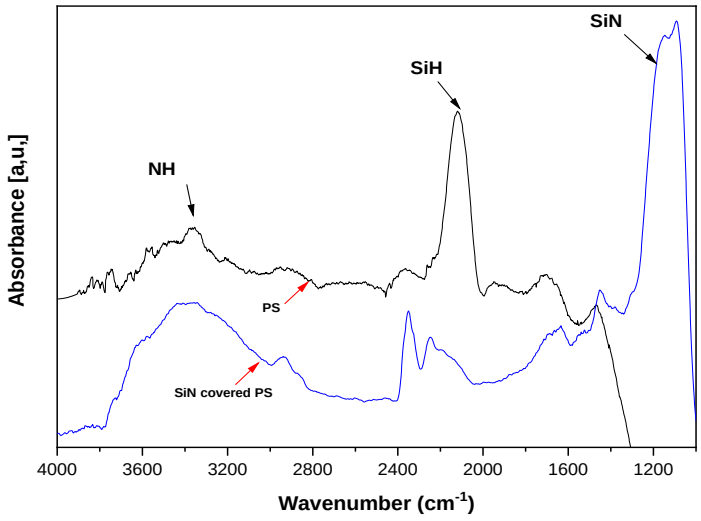

Figure 6. FT-IR characterization of mc-Si treated PS with and without SiN.

 doi:10.20944/preprints202503.1252.v1

FTIR spectra of PS and PS Covered-SiN are presented in Figure 6. The PS film shows typical structures, especially the SiH and NH stretching modes revealed at 2100 and 3300 cm^{-1}, separately, which is in agreement with the literature data [29]. A clear evolution in the absorbance spectra is observed after PS-covered-SiNx annealed at 300 °C (Figure 6b). The SiN peak that appeared at 1040 cm^{-1} is detected, along with a decrease in the intensity of the SiH peak at 2100 cm^{-1}, these factors could contribute to surface passivation and reduced reflectivity. SiH and SiN bonds are well known for their role in passivating the surface and enhancing silicon quality [30,31], as hydrogen can easily passivate dangling bonds and defects in mc-Si. As a result, this leads to an enhancement in the minority carrier diffusion length.

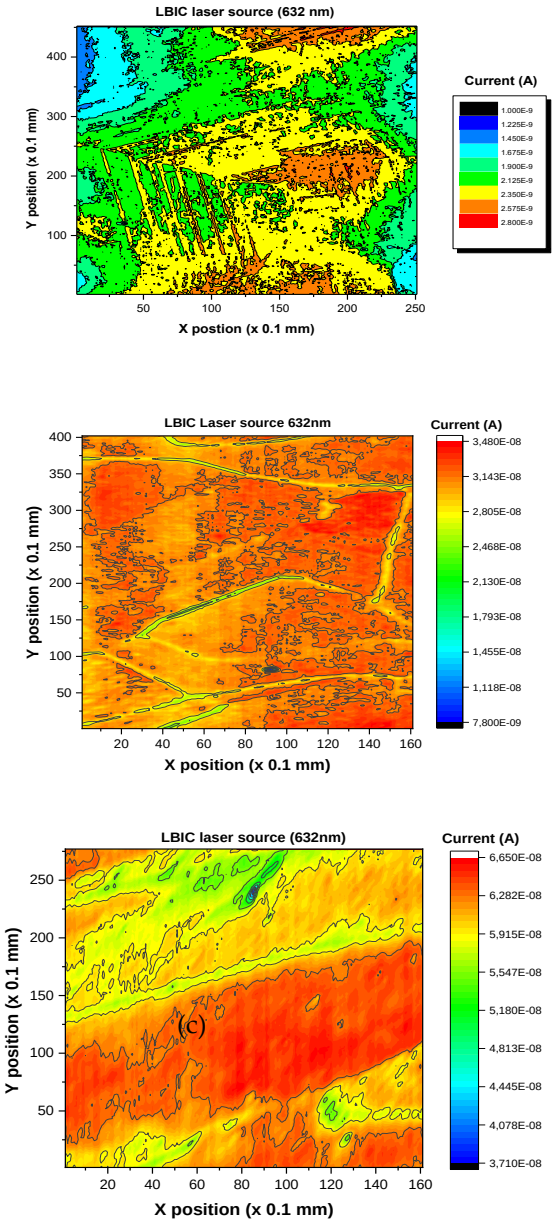

Figure 7. Two-dimension produced current LBIC distribution (a) mc-Si (b) mc-Si treated PS-Covered SiN and (b) mc-Si with Al-NPs treated porous silicon.

Figure 7 shows the Two-Dimensional Produced Current (TDPC) distribution for two samples: the first, mc-Si with Al-NPs treated porous silicon, and the second, mc-Si treated PS-Covered SiN, measured using the LBIC performance [32]. The laser beam was progressively scanned in a region of 1.5x1.5 cm2, and the TDPC was measured [33]. A significant variation in the TDPC was observed, which can be attributed to variations in the defect density. For mc-Si with aluminum-NPs treated PS, the TDPC shows an improvement compared to bare mc-Si, where the current varies between 1 and

 doi:10.20944/preprints202503.1252.v1

2.8 nA (Figure 7a). However, for mc-Si with aluminum-NPs treated porous silicon (Figure 7b), the minimum TDPC value increases to 7.8 nA, with the maximum reaching 34 nA. This improvement in TDPC is attributed to the enhancement of the minority carrier diffusion length and the passivation of recombination centers at both the grains and grain boundaries (GBs), facilitated by Si-Ox and Al-O-Si species, which passivate defects and dangling bonds on the silicon surface [33]. For the second sample, mc-Si with PS-covered SiN (Figure 7c), the minimum GC value increases to 37 nA, and the maximum reaches 66 nA, due to the well-known role of SiH and SiN bonds in passivating and improving silicon quality [30,31,34]. Overall, the obtained samples offer significant advantages in optical and optoelectronic performance compared to ref mc-Si (Table 1).

Table 1. Optical and optoelectronic performance of two samples: sample 1 (alumina nanoparticles-covered mc-Si treated PS) and ample 2 (mc-Si with PS-combined SiN).

	Reflectivity (%)	Diffusion length (μm)	Generated current (nA)
Ref mc-Si	30	2	1-2.8
Sample 1	10	100	7.8-34
Sample 2	**5**	**300**	**37-66**

5. Conclusions

The integration of silicon nitride and alumina nanoparticles demonstrates a promising approach to improving the mc-Si electronic quality for solar cell applications. The combined effects of surface passivation, defect reduction, and improved generated current contribute to enhanced solar cell efficiency. We have demonstrated that the mc-Si with PS-combined SiN_x and alumina nanoparticles-covered mc-Si treated PS substrates have several advantages for optical and optoelectronic performance. This approach leads to a dramatic decrease of the optical reflectivity to 5% for alumina nanoparticles-covered mc-Si treated PS and 10% for PS-combined SiN_x and to an enhancement of the diffusion length from 2μm to 100μm for alumina nanoparticles-covered mc-Si treated PS and 300μm for PS-combined SiN_x. However, the generated current improved from 1-2.8 nA for ref mc-Si to 7.8-34nA for alumina nanoparticles-covered mc-Si treated PS and to 37-66nA for PS-combined SiN_x. The experimental results suggest that the mc-Si with PS-combined SiN_x and alumina nanoparticles-covered mc-Si treated PS substrates induce a spectacular passivation and high electronic quality of the mc-Si surface.

Author Contributions: All authors contributed to the study's conception and design. Conceptualization, M.B.R and A.E.H.; methodology, A.M.; software, K.C.; validation, M.A.A., W.D. and M.B.R.; formal analysis, A.E.H.; investigation, A.M.; resources, K.C.; data curation, M.A.A.; writing—original draft preparation, W.D.; writing—review and editing, M.B.R.; visualization, K.C.; supervision, M.B.R.; project administration, K.C.; funding acquisition, K.C. All authors have read and agreed to the published version of the manuscript.

Funding: This work was supported and funded by the Deanship of Scientific Research at Imam Mohammad Ibn Saud Islamic University (IMSIU) (grant number IMSIU-DDRSP2502.

Data Availability Statement: The datasets generated during and/or analyzed during the current study are available from the corresponding author upon reasonable request.

Conflicts of Interest: The authors declare no conflicts of interest.

References

1. Burtescu, S., Parvulescu, C., Babarada, F., Manea, E. The low cost multicrystalline silicon solar cells. Materials Science and Engineering: B 2009), 165(3), 190-193
2. Lan, C. W., Hsu, C., & Nakajima, K. Multicrystalline silicon crystal growth for photovoltaic applications. In handbook of crystal growth 2015 pp. 373-411. Elsevier.
3. Yu, W., Xue, Y., Mei, J., Zhou, X., Xiong, M., Zhang, S. Segregation and removal of transition metal impurities during the directional solidification refining of silicon with Al-Si solvent. Journal of Alloys and Compounds 2019, 805, 198-204.
4. Lv, X., Li, H., Ding, D., Yu, X., Jin, C., & Yang, D. Interfacial characterization of non-metal precipitates at grain boundaries in cast multicrystalline silicon crystals. Journal of Crystal Growth 2025, 652, 128042.

 doi:10.20944/preprints202503.1252.v1

5. Wang, L., Liu, J., Li, Y., Wei, G., Li, Q., Fan, Z., He, D. Dislocations in Crystalline Silicon Solar Cells. Advanced Energy and Sustainability Research 2024, 5(2), 2300240.
6. Alrasheedi, N. H. The Effects of Porous Silicon and Silicon Nitride Treatments on the Electronic Qualities of Multicrystalline Silicon for Solar Cell Applications. Silicon 2024, 16(4), 1765-1773.
7. Zhou, R., Li, W., Ge, B., Song, J., Su, Q., Xi, M., & Liu, Y. Optimization of the deposited Al2O3 thin film process by RS-ALD and edge passivation applications for half-solar cells. Ceramics International 2024.
8. Chen, J., Chen, B., Lee, W., Fukuzawa, M., Yamada, M., & Sekiguchi, T. Grain boundaries in multicrystalline si. Solid State Phenomena 2010, 156, 19-26.
9. Woo, S., Bertoni, M., Choi, K., Nam, S., Castellanos, S., Powell, D. M., Choi, H. An insight into dislocation density reduction in multicrystalline silicon. Solar Energy Materials and Solar Cells 2016, 155, 88-100.
10. Jemai, A. B., Mannai, A., Khezami, L., Mokraoui, S., Algethami, F. K., Al-Ghyamah, A., Rabha, M. B. Aluminum nanoparticles passivation of multi-crystalline silicon nanostructure for solar cells applications. Silicon 2020, 12, 2755-2760.
11. Ayvazyan, G. Crystalline and Porous Silicon. In Black Silicon: Formation, Properties, and Application. Cham: Springer Nature Switzerland 2024, pp. 1-49).
12. Lipinski, M., Panek, P., Bełtowska, E., & Czternastek, H. Reduction of surface reflectivity by using double porous silicon layers. Materials Science and Engineering: B 2003, 101(1-3), 297-299.
13. Mogoda, A. S., & Farag, A. R. The effects of a few formation parameters on porous silicon production in HF/HNO3 using ag-assisted etching and a comparison with a stain etching method. Silicon 2022, 14(17), 11405-11415.
14. Rabha, M. B., Hajji, M., Mohamed, S. B., Hajjaji, A., Gaidi, M., Ezzaouia, H., Bessais, B. Stain-etched porous silicon nanostructures for multicrystalline silicon-based solar cells. The European Physical Journal-Applied Physics 2012, 57(2), 21301.
15. H Faltakh, R Bourguiga, MB Rabha, B Bessais. Superlattices and Microstructures 2012, 72: 283-295
16. M Ben Rabha, SB Mohamed, W Dimassi, M Gaidi, H Ezzaouia, B Bessais. physica status solidi c 2011, 8: 883-886
17. L Khezami, AO Al Megbel, AB Jemai, MB Rabha Applied Surface Science 2015, 353:106-111
18. Harbeke, G., Jastrzebski, L., J. Electrochem. Soc 1990, 137: 696–699
19. M. Ben Rabha, M. Salem, M.A. El Khakani, B. Bessais, M. Gaidi, Mater. Sci. Eng.B 2013, 178: 695–697
20. A. Cuevas, D. Mcdonald, Sol. Energy 2004, 76: 255–262
21. Lotfi Khezami, Abdelbasset Bessadok Jemai, Raed Alhathlool, Mohamed Ben Rabha Solar Energy 2016, 129:38-44
22. O. Porre ; S. Martinuzzi ; M. Pasquinelli ; I. Perichaud ; N. Gay.Published in: Conference Record of the Twenty Fifth IEEE Photovoltaic Specialists Conference 1996
23. F.A. Harraz, T. Sakka, Y.H. Ogata, Phys. Status Solidi (A) 2003, 197, 51-56
24. M. Rahmani, A. Moadhen, M.A. Zaibi, H. Elhouichet, M. Oueslati, J. Lumin 2008, 128,1763-1766
25. W.M. Arnoldbik, F.H.P.M. Habraken, Nucl. Instrum. Methods Phys. Res. B 2007, 256-300
26. Y. Kanemitsu, S. Okamoto, Phys. Rev. B 1997, 56: 1696
27. T. Maruyama, S. Ohtani, Appl. Phys. Lett 1994, 65: 1346
28. Yoshihiko Kanemitsu, Toshiro Futagi, Takahiro Matsumoto, and Hidenori Mimura. Phys. Rev. B 1994,49: 14732
29. B. Stannowski, J. K. Rath, and R. E. I. Schropp, J. Appl. Phys 2003, 93, 2618
30. Lelièvre, J. F., Fourmond, E., Kaminski, A., Palais, O., Ballutaud, D., Lemiti, M. Study of the composition of hydrogenated silicon nitride SiNx: H for efficient surface and bulk passivation of silicon. Solar Energy Materials and Solar Cells 2009, 93(8), 1281-1289.
31. Dao, V. A., Heo, J., Kim, Y., Kim, K., Lakshminarayan, N.,Yi, J. Optimized surface passivation of n and p type silicon wafers using hydrogenated SiNx layers. Journal of non-crystalline solids 2010, 356, 2880-2883.
32. Dimassi, W., Derbali, L., Bouaı¨cha, M., Bessaıs, B., Ezzaouia, H. Two-dimensional LBIC and Internal-Quantum-Efficiency investigations of grooved grain boundaries in multicrystalline silicon solar cells. Sol. Energy 2011, 85, 350–355.

 doi:10.20944/preprints202503.1252.v1

33. Ben Rabha, M., Dimassi, W., Bouaicha, M., Ezzaouia, H., Bessais, B. Laser-beam-induced current mapping evaluation of porous silicon-based passivation in polycrystalline silicon solar cells. Sol. Energy 2009, 83, 721.
34. Achref, M., Khezami, L., Mokraoui, S., Rabha, M. B. Effective surface passivation on multi-crystalline silicon using aluminum/porous silicon nanostructures. Surfaces and Interfaces 2020, 18, 100391.
35. Krotkus, A., Grigoras, K., Pacebutas, V., Barsony, I., Vazsonyi, E., Fried, M., Szlafcik, J., Nijs, J., Levy-Clement, C., 1997. Efficiency improvement by porous silicon coating of multicrystalline solar cells. Sol. Energy Mater. Sol. Cells 45, 267.